

# Revealing a 3D Fermi Surface pocket and Electron-Hole Tunneling in $\text{UTe}_2$ with Quantum Oscillations

Christopher Broyles<sup>1</sup>, Zack Rehfuss<sup>1</sup>, Hasan Siddiquee<sup>1</sup>, Kaiwen Zheng<sup>1</sup>,

Yiwei Le<sup>1</sup>, Martin Nikolo<sup>2</sup>, David Graf<sup>3</sup>, John Singleton<sup>4</sup>, Sheng Ran<sup>1</sup>

<sup>1</sup> *Department of Physics, Washington University in St. Louis, St. Louis, MO 63130, USA*

<sup>2</sup> *Department of Physics, Saint Louis University, St. Louis, MO, 63103, USA*

<sup>3</sup> *National High Magnetic Field Laboratory, Florida State University, Tallahassee, FL 32310, USA*

<sup>4</sup> *National High Magnetic Field Laboratory, Pulse Field Facility, Los Alamos National Laboratory, Los Alamos, New Mexico, 87545, USA*

Spin triplet superconductor  $\text{UTe}_2$  is widely believed to host a quasi-two-dimensional Fermi surface, revealed by first principal calculations, photoemission and quantum oscillation measurements. An outstanding question still remains as to the existence of a three-dimensional Fermi surface pocket, which is crucial for our understanding of the exotic superconducting and topological properties of  $\text{UTe}_2$ . This 3D Fermi surface pocket appears in various theoretical models with different physics origins, but has not been detected experimentally. Here for the first time we provide a concrete evidence for a relatively isotropic, small Fermi surface pocket of  $\text{UTe}_2$  via quantum oscillation measurements. In addition, we observed high frequency quantum oscillations corresponding to electron-hole tunneling between adjacent electron and hole pockets. The coexistence of 2D and 3D Fermi surface pockets, as well as the breakdown orbits, provides a test bed for theoretical models and aid the realization of a unified understanding of superconducting state of  $\text{UTe}_2$  from the first-principles approach.

Spin triplet superconductivity offers a promising route to topologically protected quantum computing, with Majorana Fermions as surface state excitations [1, 2]. The recent discovery of spin triplet superconductivity in  $\text{UTe}_2$  has prompted intense research efforts [3]. Spin triplet pairing is strongly suggested by the extremely large, anisotropic upper critical field  $H_{c2}$  [3] and the temperature independent NMR Knight shift in the superconducting state [4–6]. Time reversal symmetry breaking is indicated by the observation of finite Kerr rotation [7] as well as the chiral in-gap bound states shown by scanning tunneling spectroscopy [8]. Charge density waves have been observed in the normal state of  $\text{UTe}_2$  from scanning tunneling spectroscopy measurements [9], which develop into an unprecedented spin triplet pair density wave in the superconducting state [10].

Even more strikingly,  $\text{UTe}_2$  hosts two independent field-induced superconducting phases [11]. Embedded in a field polarized state, the higher-field superconducting phase reenters at an unusually high magnetic field of 45 T and persists up to 65 T when the magnetic field is aligned over a limited angular range about the normal direction to the (011) plane. This high-field phase greatly challenges our current understanding of superconductivity, and no theoretical explanation has emerged.

A knowledge of electronic band structure is essential in the understanding of superconducting and topological properties of  $\text{UTe}_2$ . Despite extensive efforts [12–17], a unified picture has not been achieved. A quasi-2D Fermi surface, oriented along  $k_x$  and  $k_y$ , was revealed by first-principles calculations [12–14], and supported by angle-resolved photoemission (ARPES) and de Haas van Alphen (dHvA) oscillation measurements [18, 19]. On the other hand, this large 2D Fermi surface alone does not explain various properties of  $\text{UTe}_2$ , e.g., the non-trivial

topology of the superconductivity [12, 13], the multiple superconducting states [20–22], the Fermi surface reconstruction at the metamagnetic transition [23, 24], and the nearly isotropic electronic transport [25]. This spurred searches for additional Fermi-surface sections, likely with a 3D character. A reexamination of the Kondo interaction within DFT+DMFT calculations predicted a 3D isotropic Fermi-surface pocket surrounding the  $\Gamma$ -point [17]. The electron and hole Fermi-surfaces are also reconstructed to enclose the corners of the Brillouin zone [17]. In contrast, a tight binding model approach preserves the quasi-2D structure calculated from DFT+ $U$  while introducing a new Fermi surface with 3D character at the  $k_z = \pi/2c$  plane [15]. Small Fermi-surface sections may have been observed by soft x-ray ARPES measurements [26]. However, a close examination reveals that the same data set could as well match predictions of quasi-2D Fermi surface sections, leaving the conclusions ambiguous.

Here we report quantum oscillations of  $\text{UTe}_2$  observed on high quality single crystals grown using molten salt flux method [27]. Most importantly, we provide the first concrete evidence for a relatively isotropic, small Fermi surface pocket, in addition to the quasi-2D cylindrical Fermi surface. We also observed quantum oscillations with very high frequencies, consistent with breakdown orbits due to the tunneling between electron and hole pockets. The 3D Fermi surface holds the promise for the understanding of many exotic properties of  $\text{UTe}_2$ , such as the topology of the superconducting state [17], the nature of magnetic fluctuations [15], and the mechanism of the high field induced superconductivity. Our observations apply strong constraints on the theoretical understanding of  $\text{UTe}_2$ . Any successful model of  $\text{UTe}_2$  needs to account for all three salient features: the 2D cylindrical Fermi-

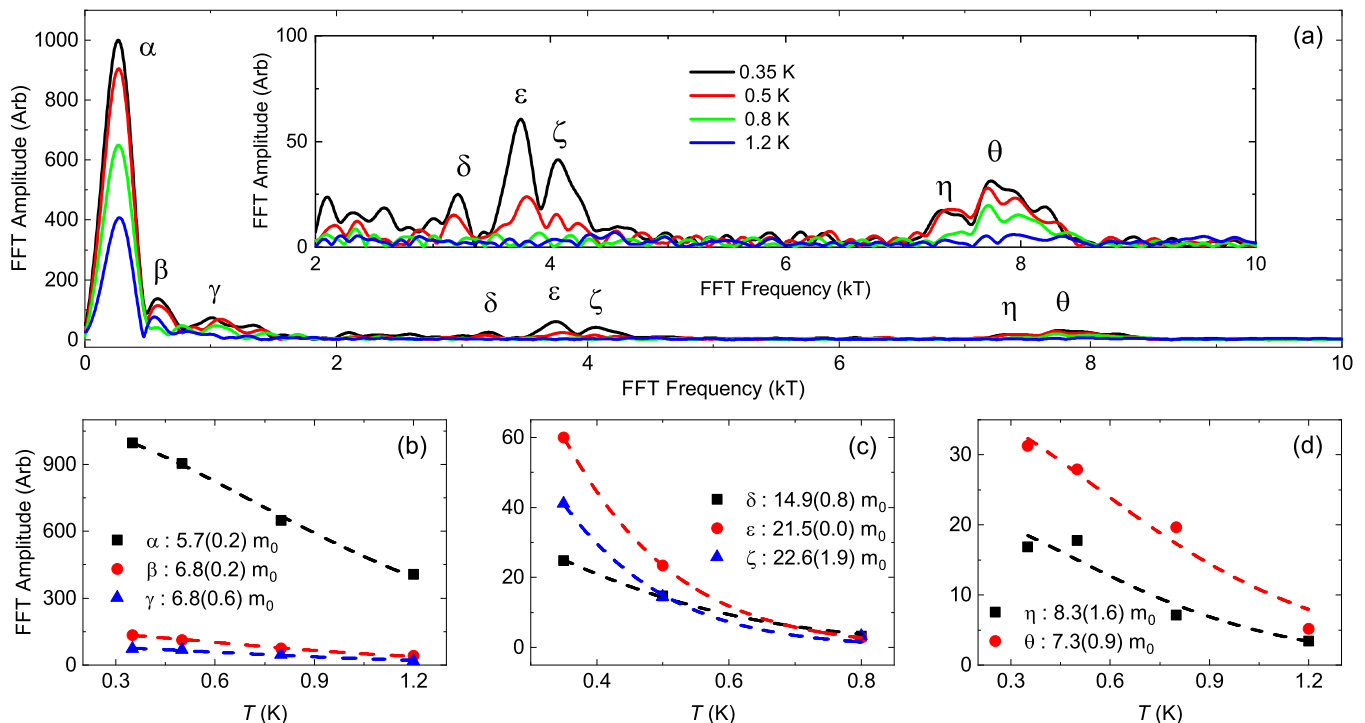


Figure 1. (a) The FFT spectrum of the background subtracted signal,  $\Delta f_{TDO}$ , is plotted for multiple temperatures, with the magnetic field oriented close to the  $c$ -axis. The inset shows the mid and high frequency peaks with better resolution. (b-d) The temperature dependent damping of the FFT peaks are fitted with Lifshitz–Kosevich formalism to calculate effective mass  $m^*$ .

surface section, small isotropic Fermi-surface sections and adjacent pockets allowing for tunneling.

The quantum oscillations of  $UTe_2$  were measured using an inductance coil as part of a tunnel diode oscillator (TDO) circuit, where the resonant frequency,  $f_{TDO}$ , is coupled to the sample magnetization and conductivity (see SI for details [41]). Figure 1a plots the fast Fourier transform (FFT) of  $\Delta f_{TDO}$  with magnetic field oriented close to the  $c$  axis. There are three groups of well resolved frequencies, below 1 kT, around 4 kT and 8 kT. As expected for magnetic quantum oscillations, the amplitudes of all of these frequencies decrease with increasing temperature, in agreement with the expectations of Fermi-Dirac statistics. The effective masses are calculated from the temperature dependent damping using the Lifshitz–Kosevich (L-K) formalism [28]. The obtained values are large for all the frequencies, in the range of 5 – 25  $m_0$ , where  $m_0$  is the mass of the free electron, consistent with heavy electronic states. Note that our base temperature, 0.35 K, is about 50 times higher than that in the previous dHvA study [19], while our magnetic field is only three times larger. Nevertheless, quantum oscillations are successfully observed, indicating the good quality of the samples used in the current study.

The mid-range frequencies around 4 kT are in a good agreement with previous dHvA oscillations seen in magnetic fields of up to 14 T [19]. These frequencies are con-

sistent with those of the GGA+ $U$  calculations with  $U = 2$  eV, which predicts quasi-2D electron and hole Fermi surfaces with a cylindrical shape [13]. Based on these calculations,  $F_\delta = 3.2$  kT corresponds to a hole pocket oriented along  $k_x$ , and  $F_\epsilon = 3.7$  kT and  $F_\zeta = 4.1$  kT to an electron pocket oriented along  $k_y$  [12, 13].

Further knowledge is gained on the topology of the Fermi surface from the angle dependence of the quantum oscillation frequencies. Here, two samples are measured: sample S1, which rotates from  $H \parallel c$  towards the  $b$ -axis, and sample S2, which rotates from  $H \parallel c$  towards the  $a$ -axis. To further confirm the rotation angle, the critical field for the metamagnetic transition was used for sample S1 and the superconducting critical field was used for sample S2, as shown in Fig. 2d. The FFT peak positions for both samples are collected in Fig. 2c, with the  $c - a$  axis rotation plotted against recent dHvA oscillations [19]. The  $c - a$  axis rotation provides good agreement, with the both electron and hole orbit showing cylindrical angle dependence. Similar cylindrical angle dependence is observed for the  $c - b$ -axis rotation in the low angle range, while the FFT peaks quickly drop to the noise level for angles above  $30^\circ$ .

Our key finding is the observation of quantum oscillations with new frequencies in two frequency ranges, below 1 kT and around 8 kT. First we investigate the frequencies around 8 kT. Figure 2a shows 2 kT high pass filtered  $\Delta f_{TDO}$  from sample S1, with a  $5^\circ$  rotation from

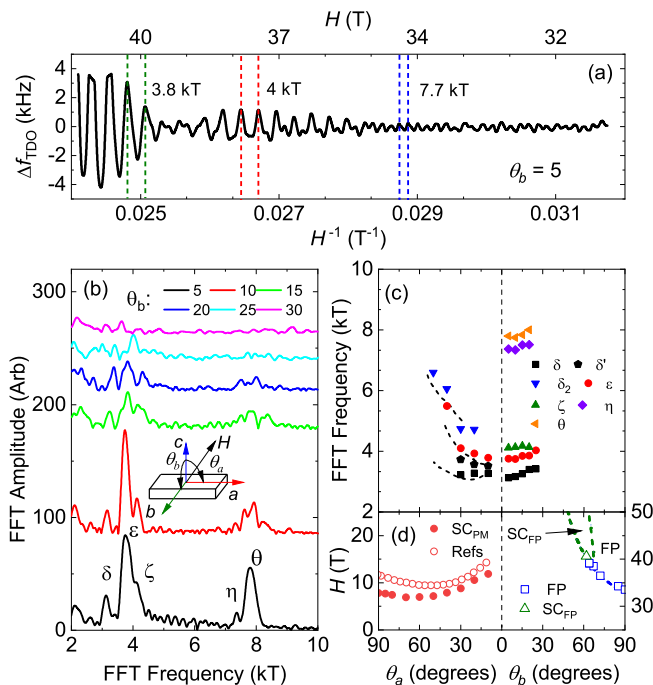


Figure 2. (a) The background subtracted signal,  $\Delta f_{res}$ , with a high pass filter of 2 kT, is plotted as a function of  $H^{-1}$ , with magnetic field oriented  $5^\circ$  from the  $c$  axis toward  $b$  axis. There are three distinct oscillations, which correspond to  $F_\epsilon$  (green),  $F_\zeta$  (red), and  $F_\theta$  (blue). (b) Multiple spectra are plotted as the magnetic field is rotated from the  $c$  axis towards  $b$  axis, indicated by  $\theta_b$ . (c) The peak position of the mid and high frequencies is plotted as the magnetic field is rotated from the  $c$  axis towards  $a$  axis (left), and from the  $c$  axis towards  $b$  axis (right). The  $c-a$  rotation is compared with literature [19], plotted with dashed lines. (d) The  $c-a$  rotation is traced with  $H_{c2}$  of the low field superconducting phase at 350 mK (solid), compared with measurements at 70 mK from literature (open) [19]. The  $c-b$  rotation is traced with the critical field of the metamagnetic transition  $H_{FP}$ , along with the phase boundaries from the literature (dashed lines) [11].

$c$  towards to the  $b$ -axis ( $\theta_b = 5$ ). Below 36 T, there is a prevalent 7.7 kT oscillation, which is shrouded by a larger magnitude 4 kT oscillation as  $H$  increases. The beating phenomenon in the high field range is due to a collection of frequencies around 4 kT. The FFT shows at least two well resolved frequencies around 8 kT. The peak position is tracked until  $\theta_b = 20$ , depicting a similar angle dependence to its mid-frequency counterparts.

A frequency of 7.7 kT would correspond to a Fermi surface area of  $0.74 \text{ \AA}^{-2}$ , which is 48% of the Brillouin zone in the  $k_x$ - $k_y$  plane. There is no experimental nor theoretical indication of such a large Fermi-surface section [12, 13, 18, 26], coexisting with the electron and hole pockets discussed above. There are a few other mechanisms that can potentially give rise to high oscillation frequencies: high order harmonics, magnetic breakdown, and quantum interference [29]. The high-frequency peaks,  $F_\eta$  and  $F_\theta$ , are close to being second

harmonics of the mid-frequency peaks. However, the temperature dependence of the  $n$ th harmonic should give an apparent effective mass that is  $n$  times the mass of the fundamental ( $n = 1$ ) frequency [28, 29]. The apparent effective masses for the high frequencies are smaller than those of the 4 kT frequencies, ruling out this possibility.

In high magnetic fields, electrons could tunnel between adjacent pockets, giving rise to new quantum oscillations in breakdown orbits [29]. Such oscillations are suppressed in amplitude by a factor  $\exp(-B/B_c)$ . The breakdown field  $B_c \propto \Delta k^2$ , with  $\Delta k$  being the gap between adjacent pockets of the Fermi surface, is typically too large for this effect to be observed in most materials. In  $\text{UTe}_2$ , adjacent pockets are close to each other in  $k$ -space, making it possible to observe new oscillations in relatively low magnetic field (starting from around 30 T). Our analysis indicates that the each of the high frequencies is roughly the addition of two frequencies in the 4 kT range, consistent with the breakdown orbits. There is an additional increase ( $\sim 400$  T) in FFT frequency corresponding to the tunneling length in  $k$ -space. Note that in case of  $\text{UTe}_2$  the tunneling happens between adjacent electron and hole pockets, in which electrons move in opposite directions. Similar electron-hole tunneling has been observed in Weyl semimetals where electron and hole pockets are close in  $k$  space [30, 31].

In Fig. 3 we present two scenarios for the tunneling. In the first case, figure of eight pattern, electrons keep the same direction when tunneling between electron and hole pockets. This tunneling is allowed by semiclassical theory. The resulting oscillation frequency of the breakdown orbit equals the difference of the involved frequencies  $f_a - f_b$  (due to the opposite enclosed areas defined by electron and hole paths, detailed in SI) and the effective mass equals the sum of the involved effective masses  $m_a + m_b$ . This is opposite to what we observed. As a matter of fact, due to the large resulting effective mass, it requires much lower temperatures to observe frequencies due to this type of tunneling. The frequency we observed,  $f = f_a + f_b$ , seems to correspond to the second case, known as Stark quantum interference, which has been observed in other materials [30, 32, 33]. This effect is due to interference between alternative quasiparticle orbits around different Fermi-surface sections that are weakly connected via tunnelling [34, 35]. The interference leads to an apparent effective mass that is the difference between the effective masses of the constituent orbits,  $m = m_a - m_b$ , in agreement with our observations (see SI [41]).

Now we turn to the other group of new frequencies. In the low frequency regime, we observed oscillations with  $F_\alpha = 270$  T,  $F_\beta = 680$  T, and  $F_\gamma = 1000$  T. The signature of the lowest frequency oscillation,  $F_\alpha$ , is prominent for both samples S1 and S2. Note that the low frequency oscillations are readily visible even in the raw data of S2, displayed in Fig. 4a. Similar oscillations for S1 are plotted in Fig. 4b and 4c, with field oriented along the  $c$ - and  $b$ -axis respectively. While  $F_\beta$  and  $F_\gamma$  peaks appear close

to the second and third harmonics of  $F_\alpha$ , the peak positions are not exact multiples. In addition, the effective mass is not consistent with the expected  $n$ th multiple. The low frequency peaks could as well come from magnetic breakdown of 4 kT orbits in the form of figure of eight. However, the effective mass would be  $m_a + m_b$ , much higher than the observed values. Therefore the low frequency oscillations must pertain to a real carrier orbit on the Fermi surface that have not been captured from previous ARPES and dHvA measurements.

The geometry of this small Fermi-surface pocket is investigated using the field-angle dependence in Fig. 4e. For a large angle range, only a few cycles of oscillations were observed, therefore we use the frequency obtained from sinusoidal fit instead of the FFT peak position to trace the angle dependence of  $F_\alpha$  (see SI for a comparison between sin fit and FFT). There is a small dip in frequency at  $\theta_b = 60^\circ$ , which is consistent for multiple field sweeps. This angle range coincides with the field induced superconducting state [11]. Other than that,  $F_\alpha$  is almost angle independent, indicating a nearly spherical Fermi-surface section. A sufficient number of cycles were observed near the  $a$ -axis, which allows to construct Landau level fan diagrams for two angles,  $\theta_a = 90^\circ$  and  $84^\circ$ , shown in Fig. 4b. The linear extrapolation for both angles show a y-intercept close to zero, indicating topologically trivial orbit.

This nearly isotropic, small Fermi-surface section provides a test bed for different theoretical models of  $\text{UTe}_2$ . First principles calculations have predicted a wide range of underlying band structures, largely due to the modeling complexity associated with  $f$ -electron strong correlations and Kondo lattice physics. Results of DFT+ $U$  and GGA+ $U$  calculations are very sensitive to the choice of  $U$  [13]. A quasi-2D Fermi surface is predicted by GGA+ $U$  for  $U = 2$  eV (DFT+ $U$  for  $U = 6$  eV), which is in a fairly good agreement with the apparent ARPES

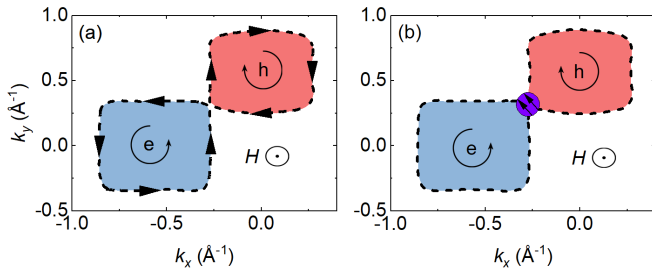


Figure 3. A cartoon diagram of the breakdown orbits due to the electron-hole tunneling between the adjacent pockets of 2D Fermi surface of  $\text{UTe}_2$ , taken from reference [13]. The orbit depicted in (a) is allowed by semi-classical theory and results in the subtraction of frequency and sum of effective mass,  $f = f_a - f_b$  and  $m = m_a + m_b$ . (b) Stark quantum interference between the orbits about the electron and hole pockets results in the sum of frequency and subtraction of effective mass,  $f = f_a + f_b$  and  $m = m_a - m_b$ , consistent with our observation.

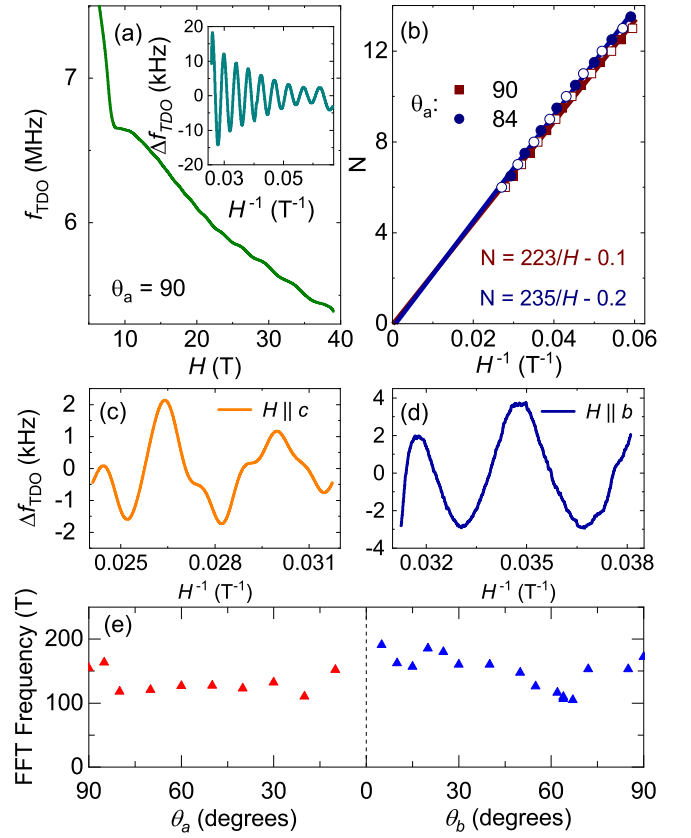


Figure 4. (a) The raw data for sample S2 TDO measurement, with magnetic field oriented along the  $a$ -axis. The inset displays the background subtracted signal. (b) The Landau Level fan diagram is constructed for two angles near the  $b$ -axis by assigning  $n + 1/2$  to maximums and  $n$  to minimums of the oscillations. The phase shift,  $\Phi$ , is calculated by extrapolating the linear fit to  $0 H^{-1}$ . The background subtracted data,  $\Delta f_{TDO}$ , with a low pass filter of 2 kT, for sample S1 is plotted for magnetic field oriented along (c) the  $c$ -axis and (d) along the  $b$ -axis. (e) The peak position of the low frequencies is plotted as the magnetic field is rotated from the  $c$  axis towards  $a$  axis (left), and from the  $c$  axis towards  $b$  axis (right).

observation of rectangular pockets and dHvA oscillations of 4 kT frequency [18, 19]. A topological Lifshitz transition occurs as  $U$  decreases [13]. When  $U$  is decreased to 1.0 eV, GGA+ $U$  calculations predict a tiny electron pocket appearing at the Brillouin zone boundary around the  $X$  point and a tiny hole pocket around the  $R$  point. These small Fermi-surface sections could potentially correspond to the low frequencies we observed. However, for  $U = 1.0$  eV, the large cylindrical Fermi surface no longer exists. It is not clear whether fine tuning of  $U$  could lead to both small and large Fermi-surface pockets that we observed.

Another possible origin for the small Fermi-surface section is suggested by a recent DFT + DMFT calculations, considering Kondo interaction induced Fermi-surface reconstruction [17]. At low temperatures, due to the Kondo resonance, the original quasi-2D Fermi surface

morphs into another quasi-2D Fermi-surface section surrounding the Brillouin zone corners and a 3D small Fermi pocket closing the  $\Gamma$  point. The renormalized bands are not accessible to the ARPES measurements as they are expected to emerge below 10 K. At the first glance, the presences of both large 2D and small 3D Fermi-surface sections could be responsible for the frequencies we observed. However, the renormalized 2D Fermi-surface section no longer has pockets close in the  $k$ -space, leaving the electron-hole tunneling impossible. It would require additional mechanism to explain the frequencies we observed around 8 kT.

The most promising route might be the tight binding model [15], based on the results of DFT+ $U$  calculations with an intermediate  $U$ . The 2D cylindrical Fermi-surface section is preserved in this model. In the meantime, due to the contribution of itinerant  $f$ -electrons, the hole Fermi-surface section is bent and encloses the  $X$ -point. It is conceivable that when hybridization between the Te  $5p$ -orbital of the hole pocket and the U  $5f$ -orbital is turned on, a gap will open and isolated small pockets will form around  $X$ -point that are almost spherical. In this scenario, 4 kT frequencies from 2D cylindrical Fermi-surface sections, 8 kT frequencies from tunneling between electron and hole pockets, as well as low frequencies from small Fermi-surface pockets, could all be captured in one model. Further theoretical investigation is required to verify this hypothesis.

Our observation of the 3D Fermi-surface pocket is crucial for the understanding of the exotic properties of  $\text{UTe}_2$ . Although the new small Fermi-surface section itself has trivial topology, it could still give rise to a nontrivial topology of superconductivity. Both GGA+ $U$  and DFT+ $U$  calculations predict a topologically trivial superconducting state for the 2D cylindrical Fermi surface [12, 13]. The addition of a 3D Fermi surface changes the occupation number at time-reversal invariant momenta, which in turn changes the winding number and could potentially lead to topological superconductiv-

ity [36, 37]. In addition, new 3D Fermi surface might be responsible for the magnetic fluctuations and multiple order parameters observed in  $\text{UTe}_2$ . In the tight binding model, the appearance of Fermi surface at  $k_z$  plan enhances ferromagnetic fluctuations, rather than antiferromagnetic ones, and extends the odd-parity symmetry from  $B_{iu}$  to include the  $A_u$  point-group, which transforms to the even-parity  $A_g$  state under pressure [15]. This makes the small Fermi surface sections key to the understanding of multiple superconducting states under pressure and the overall  $P$ - $T$  phase diagram [20–22, 38–40]. Another open question about  $\text{UTe}_2$  is the origin of the high-field superconducting phase existing inside the field-polarized state. Upon the metamagnetic transition into the field polarized state, a Fermi-surface reconstruction has been suggested by the thermopower experiments [23, 24], which likely involves a small, rather than large, Fermi-surface section. It is crucial to investigate how the small Fermi-surface pocket we observed here changes upon the metamagnetic transition, which is an undergoing project.

To summarize, we provide concrete evidence for a small 3D Fermi-surface section in  $\text{UTe}_2$  via quantum oscillations measurements, owing to the large magnetic field range in this study. The 3D small Fermi-surface pocket is crucial for our understanding of various exotic properties of  $\text{UTe}_2$ : nontrivial topological superconductivity, multiple order parameters, and the extremely high-field-induced superconducting state. Together with the observation of electron-hole tunneling, this discovery applies strong constraints to theoretical models, aiding the eventual realization of a unified understanding of the superconducting states of  $\text{UTe}_2$ .

We would like to thank Andrew Wray, Yifeng Yang, Daniel Agterberg, Carlo Beenakker and Li Yang for fruitful discussions. Research at the National High Magnetic Field Laboratory NHMFL was supported by NSF Cooperative Agreement No. DMR-1644779 and the State of Florida. JS thanks the DOE BED FWP *Science of 100 T* for support.

- 
- [1] M. Sato and Y. Ando, Topological superconductors: a review, *Reports on Progress in Physics* **80**, 076501 (2017).
  - [2] C. Kallin and J. Berlinsky, Chiral superconductors, *Reports on Progress in Physics* **79**, 054502 (2016).
  - [3] S. Ran, C. Eckberg, Q.-P. Ding, Y. Furukawa, T. Metz, S. R. Saha, I.-L. Liu, M. Zic, H. Kim, J. Paglione, and N. P. Butch, Nearly ferromagnetic spin-triplet superconductivity, *Science* **365**, 684 (2019).
  - [4] G. Nakamine, S. Kitagawa, K. Ishida, Y. Tokunaga, H. Sakai, S. Kambe, A. Nakamura, Y. Shimizu, Y. Homma, D. Li, F. Honda, and D. Aoki, Superconducting properties of heavy fermion  $\text{UTe}_2$  revealed by  $^{125}\text{Te}$ -nuclear magnetic resonance, *Journal of the Physical Society of Japan* **88**, 113703 (2019).
  - [5] G. Nakamine, K. Kinjo, S. Kitagawa, K. Ishida, Y. Tokunaga, H. Sakai, S. Kambe, A. Nakamura, Y. Shimizu, Y. Homma, D. Li, F. Honda, and D. Aoki, Anisotropic response of spin susceptibility in the superconducting state of  $\text{UTe}_2$  probed with  $^{125}\text{Te}$ -NMR measurement, *Phys. Rev. B* **103**, L100503 (2021).
  - [6] H. Fujibayashi, G. Nakamine, K. Kinjo, S. Kitagawa, K. Ishida, Y. Tokunaga, H. Sakai, S. Kambe, A. Nakamura, Y. Shimizu, Y. Homma, D. Li, F. Honda, and D. Aoki, Superconducting order parameter in  $\text{UTe}_2$  determined by Knight Shift measurement, *Journal of the Physical Society of Japan* **91**, 043705 (2022).
  - [7] I. M. Hayes, D. S. Wei, T. Metz, J. Zhang, Y. S. Eo, S. Ran, S. R. Saha, J. Collini, N. P. Butch, D. F. Agterberg, A. Kapitulnik, and J. Paglione, Multicomponent superconducting order parameter in  $\text{UTe}_2$ , *Science* **373**, 797 (2021).
  - [8] L. Jiao, S. Howard, S. Ran, Z. Wang, J. O. Rodriguez,

- M. Sigrist, Z. Wang, N. P. Butch, and V. Madhavan, Chiral superconductivity in heavy-fermion metal  $UTe_2$ , *Nature* **579**, 523 (2020).
- [9] A. Aishwarya, J. May-Mann, A. Raghavan, L. Nie, M. Romanelli, S. Ran, S. R. Saha, J. Paglione, N. P. Butch, E. Fradkin, *et al.*, Magnetic-field sensitive charge density wave orders in the superconducting phase of  $UTe_2$ , *arXiv preprint* **2207**, 09491 (2022).
- [10] Q. Gu, J. P. Carroll, S. Wang, S. Ran, C. Broyles, H. Siddiquee, N. P. Butch, S. R. Saha, J. Paglione, J. Davis, *et al.*, Detection of a pair density wave state in  $UTe_2$ , *arXiv preprint* **2209**, 10859 (2022).
- [11] S. Ran, I.-L. Liu, Y. S. Eo, D. J. Campbell, P. M. Neves, W. T. Fuhrman, S. R. Saha, C. Eckberg, H. Kim, D. Graf, *et al.*, Extreme magnetic field-boosted superconductivity, *Nature Physics* **15**, 1250 (2019).
- [12] Y. Xu, Y. Sheng, and Y.-f. Yang, Quasi-two-dimensional fermi surfaces and unitary spin-triplet pairing in the heavy fermion superconductor  $UTe_2$ , *Phys. Rev. Lett.* **123**, 217002 (2019).
- [13] J. Ishizuka, S. Sumita, A. Daido, and Y. Yanase, Insulator-metal transition and topological superconductivity in  $UTe_2$  from a first-principles calculation, *Phys. Rev. Lett.* **123**, 217001 (2019).
- [14] T. Shishidou, H. G. Suh, P. M. R. Brydon, M. Weinert, and D. F. Agterberg, Topological band and superconductivity in  $UTe_2$ , *Phys. Rev. B* **103**, 104504 (2021).
- [15] J. Ishizuka and Y. Yanase, Periodic anderson model for magnetism and superconductivity in  $ute_2$ , *Phys. Rev. B* **103**, 094504 (2021).
- [16] B. Kang, S. Choi, and H. Kim, Orbital selective kondo effect in heavy fermion superconductor  $UTe_2$ , *npj Quantum Materials* **7**, 64 (2022).
- [17] H. C. Choi, S. H. Lee, and B.-J. Yang, Correlated normal state fermiology and topological superconductivity in  $UTe_2$ , *arXiv preprint* **2206**, 04876 (2022).
- [18] L. Miao, S. Liu, Y. Xu, E. C. Kotta, C.-J. Kang, S. Ran, J. Paglione, G. Kotliar, N. P. Butch, J. D. Denlinger, and L. A. Wray, Low energy band structure and symmetries of  $UTe_2$  from angle-resolved photoemission spectroscopy, *Phys. Rev. Lett.* **124**, 076401 (2020).
- [19] D. Aoki, H. Sakai, P. Opletal, Y. Tokiwa, J. Ishizuka, Y. Yanase, H. Harima, A. Nakamura, D. Li, Y. Homma, Y. Shimizu, G. Knebel, J. Flouquet, and Y. Haga, First observation of the de Hass-van Alphen effect and fermi surfaces in the unconventional superconductor  $UTe_2$ , *Journal of the Physical Society of Japan* **91**, 083704 (2022).
- [20] S. Ran, H. Kim, I.-L. Liu, S. R. Saha, I. Hayes, T. Metz, Y. S. Eo, J. Paglione, and N. P. Butch, Enhancement and reentrance of spin triplet superconductivity in  $UTe_2$  under pressure, *Phys. Rev. B* **101**, 140503 (2020).
- [21] S. M. Thomas, F. B. Santos, M. H. Christensen, T. Asaba, F. Ronning, J. D. Thompson, E. D. Bauer, R. M. Fernandes, G. Fabbris, and P. F. S. Rosa, Evidence for a pressure-induced antiferromagnetic quantum critical point in intermediate-valence  $UTe_2$ , *Science Advances* **6**, eabc8709 (2020).
- [22] D. Braithwaite, M. Vališka, G. Knebel, G. Lapertot, J.-P. Brison, A. Pourret, M. Zhitomirsky, J. Flouquet, F. Honda, and D. Aoki, Multiple superconducting phases in a nearly ferromagnetic system, *Communications Physics* **2**, 147 (2019).
- [23] Q. Niu, G. Knebel, D. Braithwaite, D. Aoki, G. Lapertot, G. Seyfarth, J.-P. Brison, J. Flouquet, and A. Pourret, Fermi-surface instability in the heavy-fermion superconductor  $UTe_2$ , *Phys. Rev. Lett.* **124**, 086601 (2020).
- [24] Q. Niu, G. Knebel, D. Braithwaite, D. Aoki, G. Lapertot, M. Vališka, G. Seyfarth, W. Knafo, T. Helm, J.-P. Brison, J. Flouquet, and A. Pourret, Evidence of fermi surface reconstruction at the metamagnetic transition of the strongly correlated superconductor  $UTe_2$ , *Phys. Rev. Res.* **2**, 033179 (2020).
- [25] Y. S. Eo, S. Liu, S. R. Saha, H. Kim, S. Ran, J. A. Horn, H. Hodovanets, J. Collini, T. Metz, W. T. Fuhrman, A. H. Nevidomskyy, J. D. Denlinger, N. P. Butch, M. S. Fuhrer, L. A. Wray, and J. Paglione, *c*-axis transport in  $UTe_2$ : Evidence of three-dimensional conductivity component, *Phys. Rev. B* **106**, L060505 (2022).
- [26] S.-i. Fujimori, I. Kawasaki, Y. Takeda, H. Yamagami, A. Nakamura, Y. Homma, and D. Aoki, Electronic structure of  $UTe_2$  studied by photoelectron spectroscopy, *Journal of the Physical Society of Japan* **88**, 103701 (2019).
- [27] H. Sakai, P. Opletal, Y. Tokiwa, E. Yamamoto, Y. Tokunaga, S. Kambe, and Y. Haga, Single crystal growth of superconducting  $UTe_2$  by molten salt flux method, *Phys. Rev. Mater.* **6**, 073401 (2022).
- [28] D. Shoenberg, Theory of the de haas-van alphen effect, *Journal of Physics F: Metal Physics* **18**, 49 (1988).
- [29] D. Shoenberg, *Magnetic oscillations in metals* (Cambridge university press, 2009).
- [30] M. R. van Delft, S. Pezzini, T. Khouri, C. S. A. Müller, M. Breitzkreiz, L. M. Schoop, A. Carrington, N. E. Hussey, and S. Wiedmann, Electron-hole tunneling revealed by quantum oscillations in the nodal-line semimetal HfSiS, *Phys. Rev. Lett.* **121**, 256602 (2018).
- [31] T. E. O'Brien, M. Diez, and C. W. J. Beenakker, Magnetic breakdown and klein tunneling in a type-II Weyl semimetal, *Phys. Rev. Lett.* **116**, 236401 (2016).
- [32] T. Sasaki, H. Sato, and N. Toyota, Magnetic breakdown effect in organic superconductor  $\kappa$ -(BEDT-TTF) $_2$ Cu(NCS) $_2$ , *Solid State Communications* **76**, 507 (1990).
- [33] N. Harrison, J. Caulfield, J. Singleton, P. H. P. Reinders, F. Herlach, W. Hayes, M. Kurmoo, and P. Day, Magnetic breakdown and quantum interference in the quasi-two-dimensional superconductor in high magnetic fields, *Journal of Physics: Condensed Matter* **8**, 5415 (1996).
- [34] R. W. Stark and R. Reifenberger, Quantitative theory for the quantum interference effect in the transverse magnetoresistance of pure magnesium, *Journal of Low Temperature Physics* **26**, 763 (1977).
- [35] D. Morrison and R. W. Stark, Two-lifetime model calculations of the quantum interference dominated transverse magnetoresistance of magnesium, *Journal of Low Temperature Physics* **45**, 531 (1981).
- [36] M. Sato, Topological odd-parity superconductors, *Phys. Rev. B* **81**, 220504 (2010).
- [37] L. Fu and E. Berg, Odd-parity topological superconductors: Theory and application to  $Cu_xBi_2Se_3$ , *Phys. Rev. Lett.* **105**, 097001 (2010).
- [38] W.-C. Lin, D. J. Campbell, S. Ran, I.-L. Liu, H. Kim, A. H. Nevidomskyy, D. Graf, N. P. Butch, and J. Paglione, Tuning magnetic confinement of spin-triplet superconductivity, *npj Quantum Materials* **5**, 68 (2020).
- [39] S. Ran, S. R. Saha, I.-L. Liu, D. Graf, J. Paglione, and N. P. Butch, Expansion of the high field-boosted superconductivity in  $UTe_2$  under pressure, *npj Quantum Materials* **6**, 75 (2021).

- [40] D. V. Ambika, Q.-P. Ding, K. Rana, C. E. Frank, E. L. Green, S. Ran, N. P. Butch, and Y. Furukawa, Possible coexistence of antiferromagnetic and ferromagnetic spin fluctuations in the spin-triplet superconductor  $\text{Ute}_2$  revealed by  $^{125}\text{Te}$  NMR under pressure, *Phys. Rev. B* **105**, L220403 (2022).
- [41] See Supplementary Materials for information on the TDO method, quantum oscillations, and breakdown orbits, which includes refs. [42-45].
- [42] T. Coffey, Z. Bayindir, J. F. DeCarolis, M. Bennett, G. Esper, and C. C. Agosta, Measuring radio frequency properties of materials in pulsed magnetic fields with a tunnel diode oscillator, *Review of Scientific Instruments* **71**, 4600 (2000).
- [43] C. T. Van Degrift, Tunnel diode oscillator for 0.001 ppm measurements at low temperatures, *Review of Scientific Instruments* **46**, 599 (1975).
- [44] At the high magnetic fields applied in this study to  $\text{UTe}_2$ , the magnetic flux density  $B \approx \mu_0 H$ , the applied field.
- [45] N. Harrison, J. Caulfield, J. Singleton, P. H. P. Reinders, F. Herlach, W. Hayes, M. Kurmoo, and P. Day, Magnetic breakdown and quantum interference in the quasi-two-dimensional superconductor in high magnetic fields, *Journal of Physics: Condensed Matter* **8**, 5415 (1996).